Arabidopsis ULTRAVIOLET-B-INSENSITIVE4 Maintains Cell Division Activity by Temporal Inhibition of the Anaphase-Promoting Complex/Cyclosome [C][W]

Jefri Heyman[a,b], Hilde Van den Daele[a,b], Kevin De Wit[a,b], Véronique Boudolf[a,b], Barbara Berckmans[a,b], Aurine Verkest[a,b], Claire Lessa Alvim Kamei[a,b], Geert De Jaeger[a,b], Csaba Koncz[c,d], and Lieven De Veylder[a,b,1]

[a] Department of Plant Systems Biology, VIB, B–9052 Ghent, Belgium
[b] Department of Plant Biotechnology and Bioinformatics, Ghent University, B–9052 Ghent, Belgium
[c] Max-Planck-Institut für Züchtungsforschung, D–50829 Cologne, Germany
[d] Institute of Plant Biology, Biological Research Center of Hungarian Academy of Sciences, H–6723 Szeged, Hungary

The anaphase-promoting complex/cyclosome (APC/C) is a multisubunit ubiquitin ligase that regulates progression through the cell cycle by marking key cell division proteins for destruction. To ensure correct cell cycle progression, accurate timing of APC/C activity is important, which is obtained through its association with both activating and inhibitory subunits. However, although the APC/C is highly conserved among eukaryotes, no APC/C inhibitors are known in plants. Recently, we have identified ULTRAVIOLET-B-INSENSITIVE4 (UVI4) as a plant-specific component of the APC/C. Here, we demonstrate that UVI4 uses conserved APC/C interaction motifs to counteract the activity of the CELL CYCLE SWITCH52 A1 (CCS52A1) activator subunit, inhibiting the turnover of the A-type cyclin CYCA2;3. *UVI4* is expressed in an S phase-dependent fashion, likely through the action of E2F transcription factors. Correspondingly, *uvi4* mutant plants failed to accumulate CYCA2;3 during the S phase and prematurely exited the cell cycle, triggering the onset of the endocycle. We conclude that UVI4 regulates the temporal inactivation of APC/C during DNA replication, allowing CYCA2;3 to accumulate above the level required for entering mitosis, and thereby regulates the meristem size and plant growth rate.

INTRODUCTION

Unidirectional and irreversible progression through the cell cycle is mediated through the selective proteolytic regulation of both positive and negative regulators of cyclin-dependent kinases (CDKs). Cyclins, cell cycle inhibitors, and many other proteins are marked with ubiquitin by E3 ubiquitin ligases and, subsequently, recognized and destroyed by the 26S proteasome (Hershko, 1997; Peters, 2002). Two related E3 ubiquitin-ligase complexes are most intimately dedicated to basic cell cycle regulation, namely Skp1-Cullin-F-box (SCF)-related complexes and the anaphase-promoting complex/cyclosome (APC/C), which operate at the G1-to-S transition and in the M-G1 phases, respectively (Marrocco et al., 2010).

The APC/C is a multisubunit complex that is highly conserved among eukaryotes, consisting of at least 11 different subunits, including a catalytic core composed of APC2 and APC11 (Page and Hieter, 1999; Tang et al., 2001). Besides this core, the APC/C requires essential subunits for its activation, including the docking factor APC10/Doc1 (Destruction of D-box) and the CDC20/Fizzy or CDH1/Fizzy-related (FZR) activator subunits. Both
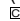
CDC20 and CDH1 activators confer substrate specificity, in part by their different activation timing and by the recognition of distinct destruction degrons, including the D-box (RxxLxxxxN), KEN-box (KENxxxE/D/N), and GxEN-box (Pfleger and Kirschner, 2000; Castro et al., 2003; Lénárt and Peters, 2006).
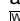
In addition to activators, the APC/C is controlled by inhibitory proteins. Such inhibitors have been described for different species. In *Homo sapiens*, *Mus musculus*, and *Xenopus laevis*, the Early mitotic inhibitor1 (Emi1), known as Regulator of cyclin A1 (Rca1) in *Drosophila melanogaster*, inhibits APC/C[CDH1] activity by operating as a pseudosubstrate (Di Fiore and Pines, 2007). Expression of *Emi1* is regulated by E2F transcription factors at the G1-to-S transition, restricting the APC/C[CDH1] activity to the interphase and allowing the accumulation of the APC/C[CDH1] targets, such as geminin and A- and B-type cyclins, during the late G1 and early S phases (Hsu et al., 2002; Verschuren et al., 2007; Tategu et al., 2008). *Xenopus* extracts depleted from Emi1 refrain from entering mitosis, because they do not accumulate mitotic cyclins (Reimann et al., 2001). Likewise, *Drosophila rca1* mutants fail to accumulate A-type cyclins and arrest in G2 (Grosskortenhaus and Sprenger, 2002). Similarly, in budding yeast (*Saccharomyces cerevisiae*), APC/C[CDH1] modulator1 (Acm1) suppresses degradation of mitotic cyclins by acting as a pseudosubstrate of APC/C[CDH1], although it is unrelated in sequence to Emi1 and Rca1 (Burton et al., 2011). Based on sequence identity, no proteins orthologous to Emi1/Rca1 or Acm1 have been recognized in plants.

The genome of *Arabidopsis thaliana* encodes three CDH1/FZR-related proteins, annotated as the *CELL CYCLE SWITCH 52*

genes (*CCS52A1*, *CCS52A2*, and *CCS52B*) (Cebolla et al., 1999). Whereas the function of CCS52B is unclear, both CCS52A1 and CCS52A2 have been implicated in the control of endocycle onset in different species (Cebolla et al., 1999; Lammens et al., 2008; Narbonne-Reveau et al., 2008; Mathieu-Rivet et al., 2010). The endoreduplication cycle represents an alternative to the mitotic cell cycle, during which mitosis is completely repressed and DNA re-replication is stimulated, resulting in a stepwise doubling of the DNA content. Whereas this phenomenon occurs only in certain cell types in mammals, endoreduplication is widespread among plants, particularly in angiosperms, in which it might occur in most cell types except gametes, meristematic tissues, and guard cells (Ullah et al., 2009). In plants, the onset of endoreduplication is often coupled to cell differentiation, because it coincides with the switch from the proliferation to the differentiation program (Beemster et al., 2005; Inzé and De Veylder, 2006). Furthermore, in *Arabidopsis*, it plays a decisive role in determining differentiation of leaf trichome precursor cells (Bramsiepe et al., 2010).

Major efforts have advanced our understanding of how plants exit the mitotic cell cycle and switch to the endocycle. Among others, cell cycle proteins important for the timing of endocycle onset in *Arabidopsis* include the A-type cyclin CYCA2;3 and the plant-specific B-type CDK CDKB1;1, which, as a complex, repress the exit from the mitotic cell cycle (Imai et al., 2006; Boudolf et al., 2009). Recently, the cyclin CYCA2;3 has been identified as one of the targets of the APC/C^{CCS52A1} in the root cell elongation zone, hinting at a role in the regulation of the endocycle by preventing an increase in CYCA2;3-CDKB1;1 activity at the G2-to-M transition (Boudolf et al., 2009).

Through tandem affinity purification (TAP), we purified the subunits of the *Arabidopsis* APC/C, revealing the presence of plant-specific binding partners (Van Leene et al., 2010), including ULTRAVIOLET-B INSENSITIVE4 (UVI4), which has been demonstrated previously to affect endoreduplication in leaves (Hase et al., 2006). Similarly, the UVI4 homolog OMISSION OF SECOND DIVISION (OSD1) was found to be an APC/C subunit (Van Leene et al., 2010) and has been proposed to regulate the oscillations of CDK activity that are required to progress through the meiosis I-to-meiosis II transition during pollen gamete formation (d'Erfurth et al., 2009, 2010; Bulankova et al., 2010). Here, we demonstrate that UVI4 regulates the APC/C activity through binding to the CCS52A activator subunits. UVI4 is likely under the direct regulation of the E2F pathway and suppresses endocycle onset by inhibiting CYCA2;3 destruction in a timely fashion and hence regulating the meristem size. Based on structural, biochemical, and genetic data, we conclude that UVI4 is a functional homolog of Emi1, representing a plant APC/C inhibitor.

RESULTS

UVI4 Is a Part of the APC/C

By means of TAP, UVI4 had been identified as an APC/C copurifying protein (Van Leene et al., 2010). Although TAP allowed the detection of the entire composition of APC/C complexes, it did not convey any information on the direct interaction between core

subunits and associated factors. Therefore, to study the interaction of UVI4 with the different APC/C subunits in more detail, we set up a yeast two-hybrid (Y2H) interaction matrix, testing all possible interactions between 18 different APC/C subunits. Y2H interactions were analyzed with a yeast mating protocol in a microtiter plate format (Boruc et al., 2010) and by scoring for His prototrophy as output signal. Three clones could not be used as bait, because of autoactivation (APC2, APC10, and APC11), but could still be used as prey. The interaction between two proteins was considered positive when growth was more than threefold enhanced on His-lacking medium relative to the background signal (see Methods). In comparison with the robust binding among the APC/C subunits observed in the TAP assay, the number of interacting partners identified by Y2H was relatively low (for raw data of all tested interactions, see Supplemental Data Set 1 online), indicating that most APC/C subunits associate through cooperative binding. Out of the 288 tested interactions, only 14 protein pairs scored positive, including the previously identified APC2-APC11, APC10-HOBBIT (HBT), and APC7-HBT interactions (Capron et al., 2003; Eloy et al., 2006; Pérez-Pérez et al., 2008). Interestingly, in addition to the association with the APC5 scaffold protein, UVI4 also bound directly to the APC/C-activating subunit CCS52A1, implying that UVI4 binds near the APC/C catalytic site (Figure 1).

UVI4 Contains Highly Conserved Motifs Required for CCS52A1 Binding

UVI4 seems to be a plant-specific protein without sequence homology with any annotated protein. However, alignment of UVI4 with its dicot homologs identified by the PLAZA online Web tool (Proost et al., 2009) revealed the presence of many highly conserved putative APC/C interaction domains, including a D (RxxL)- and a GxEN-box. In addition, nearly all UVI4-like proteins share a C-terminal Met-Arg (MR) tail, which resembles the known Ile-Arg tail required for binding of the APC/C activator proteins to the tetratricopeptide repeat-containing subunits (Vodermaier
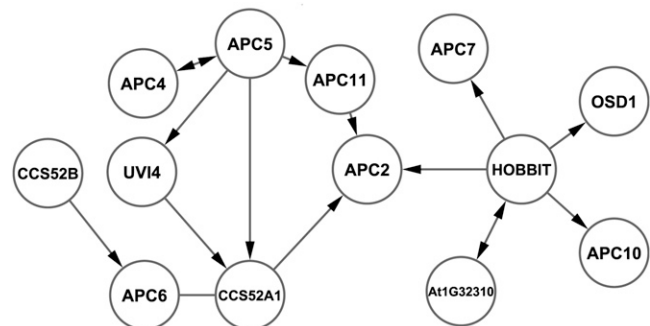

Figure 1. Y2H Interactome of APC/C Proteins.

All known APC/C subunits, including several CDC20 and CCS52 activators and recently found UVI4, OSD1, and At1G32310, were tested for binding to each other in an 18×18 matrix. Interactions were found to be positive when the OD_{600} value exceeded threefold the background value of the negative control of yeast grown in medium without His (−HIS). Arrowheads point to the interacting prey; double arrowheads indicate both interact as prey.

et al., 2003) (Figure 2A). To verify whether these domains represent true APC/C interaction motifs, a mutagenesis analysis was undertaken. For both the D-box and GxEN-box, the amino acid residues essential for APC/C binding were substituted to Ala (mD2, RxxL→AxxA; mG, GxEN→AxAA) (Figure 2B), whereas the MR tail was deleted (−MR). We also mutated a putative second D-box motif (mD1) in UVI4 that was seemingly not conserved among the different plant proteins. Subsequently, we tested the interaction of the mutant UVI4 proteins with CCS52A1 by means of the Y2H approach. In contrast with the wild-type and mD1 UVI4 proteins, the mD2, mG, and −MR mutants were unable to interact with CCS52A1, illustrating that these three mutated domains are essential for the APC/C interaction (Figure 2C).

To investigate whether different conserved domains are needed for UVI4 functionality, we tested the capacity of genes encoding the mutant alleles to complement the *uvi4* mutant phenotype. Previously, *uvi4* loss-of-function plants had been shown to display an increased DNA ploidy level because of a faster endocycle onset, correlating with an overbranched leaf trichome phenotype (Hase et al., 2006) (Figure 2D). Wild-type *Arabidopsis* trichomes have on average three branches, whereas *uvi4* leaf hairs mostly display four to five branches. The wild-type and mutant alleles of *UVI4* were cloned under the control of the *UVI4* promoter (1046 bp upstream of the start codon) and transformed into a *uvi4* loss-of-function mutant background. Wild-type *UVI4* and mutated mD1 and mD2 *uvi4* complemented the trichome phenotype, whereas plants expressing the mG or −MR alleles were not rescued (Figure 2E, Table 1). In addition to trichome branching, the DNA ploidy levels of the mature first leaves were analyzed. Complementation of the endoreduplication phenotype could be observed in *uvi4* mutants harboring the wild-type, mD1, and mD2 alleles. By contrast, no complementation could be seen in mutants transformed with the mG and −MR *uvi4* alleles (Figure 2D, Table 1). These data show that loss of the conserved GxEN-box or MR tail renders UVI4 unable to associate with the APC/C holocomplex and to exert its function.

CCS52A1 Is Required for UVI4 Activity

Our data indicated that UVI4 might regulate APC/C activity by interacting with at least the APC/C-activating subunit CCS52A1. To test this hypothesis, we generated a *uvi4 ccs52a1-1* double mutant. Mutation of *uvi4* leads to increased DNA ploidy levels, whereas *ccs52a1* mutants show decreased levels (Lammens et al., 2008). Investigation of the DNA ploidy levels of the mature first leaves of the *uvi4 ccs52a1-1* double mutant demonstrated that its ploidy distribution was more similar to that of the *ccs52a1-1* single mutant (Figure 3A), indicating that *ccs52a1-1* might be epistatic over *uvi4*. Nevertheless, endoreduplication levels in the *uvi4 ccs52a1-1* double mutant were slightly higher than those of the *ccs52a1-1* mutant (see Supplemental Table 1 online). This observation might be attributable to the regulation of endoreduplication in leaves by CCS52A2, in addition to CCS52A1 (Lammens et al., 2008). By contrast, CCS52A1 is the predominant APC/C activator involved in endocycle onset in trichomes, as illustrated by a decrease in trichome branch number and DNA content in *ccs52a1* but not in *ccs52a2* mutants (Kasili et al., 2010). When trichomes of the *uvi4 ccs52a1-1* double

mutant were examined, mainly trichomes with only two branches were detected, similar to the *ccs52a1-1* single mutant trichome phenotype (Figure 3B; see Supplemental Figure 1 online). To investigate whether the trichome branch number phenotype correlated with the DNA ploidy level of the hair cells, trichome nuclei were stained using 4′,6-diamidino-2-phenylindole (DAPI) and analyzed by epifluorescence microscopy. Mutant *uvi4* trichome nuclei were significantly larger compared with wild-type trichome nuclei, corresponding to an increased DNA content. By contrast, *ccs52a1-1* mutant trichomes contained significantly smaller nuclei compared with the wild type. In the *uvi4 ccs52a1-1* double mutant, the size of the trichome nucleus was identical to that of the *ccs52a1-1* single mutant (Figure 3C; see Supplemental Figure 2 online), indicating that *ccs52a1-1* is epistatic over *uvi4*. These data imply that the presence of the CCS52A1 activator subunit is required for UVI4 to exert its function on the APC/C activity.

UVI4 Regulates CYCA2;3 Stability

Previously, CCS52A1 had been shown to regulate CYCA2;3 abundance (Boudolf et al., 2009). Therefore, because UVI4 associates with CCS52A1, we tested whether *UVI4* deficiency affected cyclin abundance by introducing a β-estradiol-inducible *CYCA2;3-green fluorescent protein* (*GFP*) construct under control of the minimal *CaMV35S* promoter into the *uvi4* mutant background (Zuo et al., 2000; Imai et al., 2006). Two days after *CYCA2;3-GFP* induction, the GFP signal within the *Arabidopsis* root tip was assessed by confocal microscopy. A CYCA2;3-GFP signal was visible in the columella cells of control plants, but was barely detectable in the *uvi4* mutant background (Figure 4A). A decrease in CYCA2;3-GFP levels was confirmed by protein immunoblots (Figure 4B). The GFP abundance did not decrease in plants expressing a mutant allele of *CYCA2;3* harboring a mutant D-box (Figures 4A and 4B), illustrating that the increased turnover of CYCA2;3 in the *uvi4* background depended on the cyclin destruction motif.

Although no *UVI4*-overexpressing plants could be obtained, the observations made for the knockout plants could be confirmed using *Arabidopsis* cell suspension culture cells as a model system. Cultures stably co-overexpressing both *UVI4* and hemagglutinin (HA)-tagged *CYCA2;3* were generated by *Agrobacterium*-mediated transformation. As a control, cultures co-overexpressing both *CYCA2;3-HA* and the β-glucuronidase (*GUS*)-encoding gene were produced. Protein extracts were assessed for CYCA2;3 abundance by protein gel blotting with an anti-HA antibody. The CYCA2;3-HA protein was stabilized in cultures co-overexpressing *UVI4* (Figure 4D), despite the fact that the cultures accumulated only a 1.6-fold increase in *UVI4* transcripts (Figure 4E) and exhibited a 58% lower level of *CYCA2;3-HA* transcripts than in the *GUS CYCA2;3-HA* co-overexpressing culture (Figure 4F). Thus, even a minor increase in the *UVI4* transcript level is sufficient to accumulate CYCA2;3, probably because of an enhanced APC/C inhibition.

UVI4 and CDKB1;1 Synergistically Inhibit Endocycle Onset

Previously, we demonstrated that expression of a dominant negative allele of *CDKB1;1* (*CDKB1;1.N161*) induced endoreduplication, illustrating that CDKB1;1 activity drives the mitotic
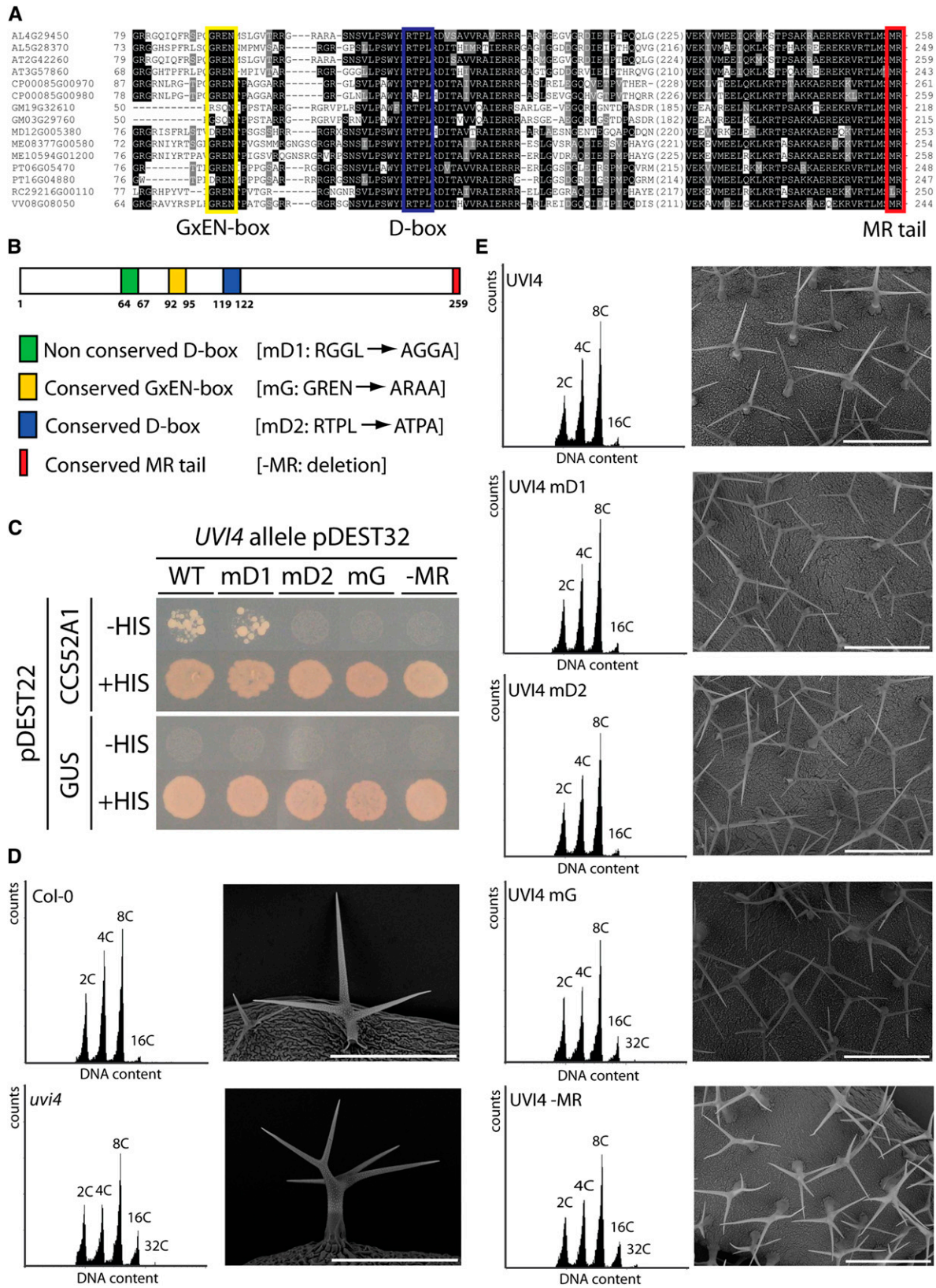
Figure 2. Structural-Functional Analysis of UVI4.

Table 1. Complementation Analysis of *uvi4* Mutants

UVI4 Allele	Independent Lines Screened	Lines Showing Complementation
Wild type	4	4
mD1	2	2
mD2	3	3
mG	3	0
−*MR*	3	0

cell cycle and suppresses endocycle onset (Boudolf et al., 2004). Ectopic expression of the CDKB1;1 binding partner *CYCA2;3* partially complemented the *CDKB1;1.N161* phenotype, suggesting that the outtitration of CYCA2;3 is at least one of the mechanisms by which *CDKB1;1.N161* induces endoreduplication (Boudolf et al., 2009). Because of the negative effect of *uvi4* on CYCA2;3 abundance, the *UVI4* deficiency would be expected to aggravate the dominant negative effect of *CDKB1;1.N161* on endoreduplication. Indeed, an increase in the DNA ploidy level of the mature first leaves was observed in the *uvi4 CDKB1;1.N161* double mutant (Figure 5; see Supplemental Table 2 online), suggesting that UVI4 and CDKB1;1 work synergistically to regulate endocycle onset.

UVI4 Inhibits Premature Cell Differentiation

CCS52A1 and CYCA2;3 antagonistically regulate the timing of cell cycle exit and endoreduplication onset (Lammens et al., 2008; Boudolf et al., 2009). As UVI4 interacts with CCS52A1 and regulates the abundance of CYCA2;3, the effects of UVI4 on the timing of cell differentiation were examined. First, we focused on the root meristem, because the cell cycle exit can be easily monitored along the proximal-distal axis, where stem cell daughters divide repeatedly before eventually starting to elongate and differentiate (Dolan et al., 1993). Root meristem size was defined as the number of cortex cells in a file extending from the quiescent center to the first elongated cortex cell (Perilli and Sabatini, 2010). A significant decrease in the number of meristematic cortex cells was observed in *uvi4* compared with wild-type 1-week-old seedlings (26 ± 4 versus 33 ± 3 cells, respectively; $P < 0.05$, Student's *t* test) (Figures 6A and 6B). By contrast, the mature cortex cell length of the two genotypes did not differ significantly (Figure 6C), with a reduced meristem size in the *uvi4* mutant as a consequence (Figure 6A). Correspondingly, measurements of root growth revealed a significant ($P < 0.05$, Student's *t* test) reduction in the *uvi4* mutant (Figure 6D). In the

uvi4 CDKB1;1.N161 double mutant, the number of meristematic cortex cells was reduced significantly ($P < 0.05$, Student's *t* test) in comparison with the single mutants (Figures 6A and 6B). Despite an increase in the cortex cell length (Figure 6C), root growth of the *uvi4 CDKB1;1.N161* double mutant was reduced significantly ($P < 0.05$, Student's *t* test) (Figure 6D).

Premature cell differentiation was observed for leaves of both *uvi4* and *CDKB1;1.N161* lines, as suggested by the reduced mature leaf cell number, resulting in a decrease in leaf size, despite a slight increase in cell size (Figures 6E to 6G). In the *uvi4 CDKB1;1.N161* double mutant, the leaf phenotype was more pronounced, again illustrating that UVI4 and CDKB1;1 synergistically inhibit cell differentiation (Figures 6E to 6G).

OSD1 Has No Direct Role in Meristem Maintenance

Because of the high level of similarity of OSD1 with UVI4 and its association with the APC/C (Van Leene et al., 2010), the *osd1-3* mutants were tested for their effect on meristem maintenance. Both diploid homozygous knockouts and their tetraploid offspring were examined, because a lack of *OSD1* provokes polyploidization in the next generation (d'Erfurth et al., 2009). Whereas the diploid *osd1-3* mutant did not differ significantly in root length, the tetraploid generation displayed a longer root (3.81 ± 0.40 cm, 3.99 ± 0.43 cm, and 4.28 ± 0.52 cm 9 d after sowing for the wild type, diploid *osd1-3*, and tetraploid *osd1-3*, respectively). At the cellular level, the diploid *osd1-3* mutants were quite similar to control plants in the number of meristematic cortex cells (33 ± 3 cells), but the tetraploid plants showed a decrease in cell number (28 ± 2 cells), which was compensated by an increase in cell size, eventually resulting in a meristem similar in size to that of control plants (Figures 7A and 7B). However, similar effects on meristem cell number (30 ± 2 cells) and size were observed in tetraploid control plants, illustrating that the observed defects were caused by the tetraploid genome rather than the absence of OSD1.

A similar conclusion could be drawn for leaf development. When examining mature leaves, diploid *osd1-3* mutants did not significantly differ in leaf size and abaxial cell number and cell size compared with the wild type (Figures 7C to 7E). By contrast, the tetraploid *osd1-3* mutant showed a significantly increased leaf size (24.6 ± 1.4 mm^2 and 31.1 ± 1.8 mm^2 for the diploid wild type and tetraploid *osd1-3*, respectively; $P < 0.001$, Student's *t* test), because of an increase in cell size (0.0012 ± 0.0001 mm^2 versus 0.0020 ± 0.0004 mm^2) and despite a decrease in cell number (16.313 ± 1.976 versus 10.033 ± 2.153). However, because the phenotypes of the tetraploid *osd1-3* mutant

---

Figure 2. (continued).

(A) Alignment of protein sequences homologous to UVI4 obtained from the PLAZA online Web tool. The conserved GxEN-box, D-box, and MR tail motifs are indicated.

(B) Schematic representation of UVI4, showing the typical APC interaction motifs and their respective amino acid substitution in the mutant alleles.

(C) Y2H interactions between wild-type (WT) and mutant UVI4 proteins and the CCS52A1 activator subunit. Interactions are positive upon growth in the absence of His (−HIS). The GUS protein was used as a negative control.

(D) and **(E)** DNA ploidy and leaf trichome complementation analysis of 21-d-old wild-type Columbia-0 (Col-0) **(D)** versus representative *uvi4* lines expressing *mD1*, *mD2*, *mG*, and −MR mutant alleles **(E)**.
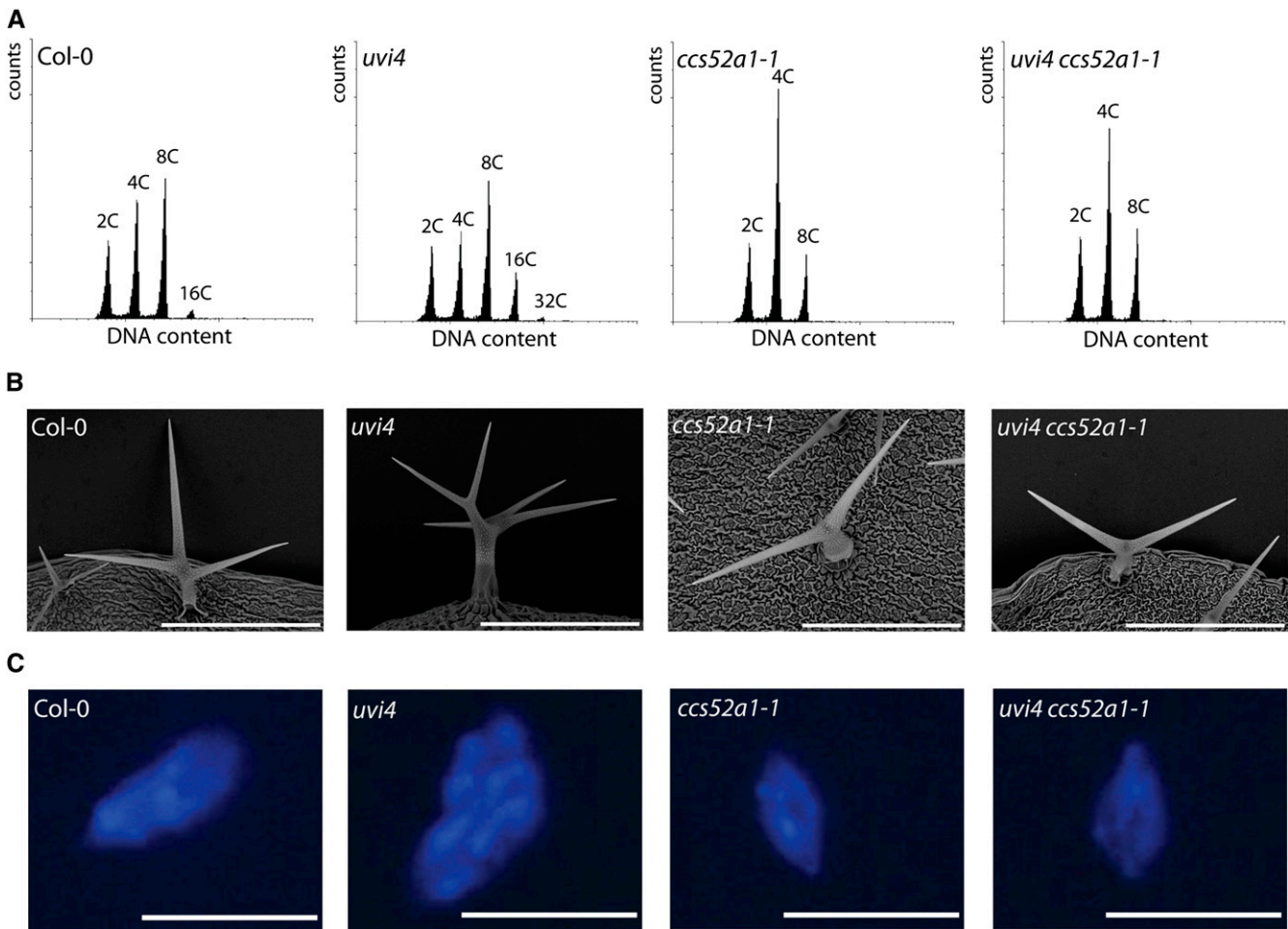
Bars in **(D)** = 300 μm; bars in **(E)** = 500 μm.

A

B

C

Figure 3. CCS52A1 Is Required for UVI4 Activity.

(A) Flow cytometric analysis of wild-type (Col-0), *uvi4*, *ccs52a1-1*, and *uvi4 ccs52a1-1* 3-week-old first leaves. Data are representative for the mean (*n* = 3).

(B) Scanning electron microscope images of wild-type (Col-0), *uvi4*, *ccs52a1-1*, and *uvi4 ccs52a1-1* trichomes.

(C) Epifluorescence images of DAPI-stained wild-type (Col-0), *uvi4*, *ccs52a1-1*, and *uvi4 ccs52a1-1* trichome nuclei. Images are representative for the mean (*n* ≥ 13).

Bars in **(B)** = 300 μm; bars in **(C)** = 25 μm.

[See online article for color version of this figure.]

resembled that of a tetraploid wild-type plant, it can be concluded that the observed cell number phenotypes only indirectly relate to OSD1 and that UVI4 plays the primary role in maintaining meristem size.

UVI4 Expression Is Regulated by E2F Transcription Factors

Expression of *UVI4-GFP* under the control of the *UVI4* promoter revealed a patchy nuclear accumulation pattern in the root tissues, indicating a cell cycle phase-specific transcription (Figure 8A). To specify the cell cycle phase in which *UVI4* was expressed predominantly, root tips were synchronized by hydroxyurea (HU) treatment (Cools et al., 2010). In this synchronized system, root tips are strongly enriched for S- and M-phase cells at the 6 h and 16 h time points, respectively. Synchronized

root tips were harvested at 2-h intervals over a total time of 22 h, and the *UVI4* expression levels were determined by reverse-transcription quantitative polymerase chain reaction (RT-qPCR). The *UVI4* transcript levels increased 4 h after the onset of synchrony, which coincides with the G1-to-S transition, peaked during the S phase at the 6 h time point, and decreased thereafter. A second peak in expression occurred at the 22 h time point, corresponding with the synchronous onset of a second S phase (Figure 8B). A similar accumulation pattern of the UVI4 protein was observed (see Supplemental Figure 3 online). These data suggest that UVI4 exerts its role as an APC/C inhibitor during the S phase.

Expression of most S phase-specific genes in *Arabidopsis* is controlled by two transcriptional activators, E2Fa and E2Fb, whose overexpression triggers the transcription of directly and
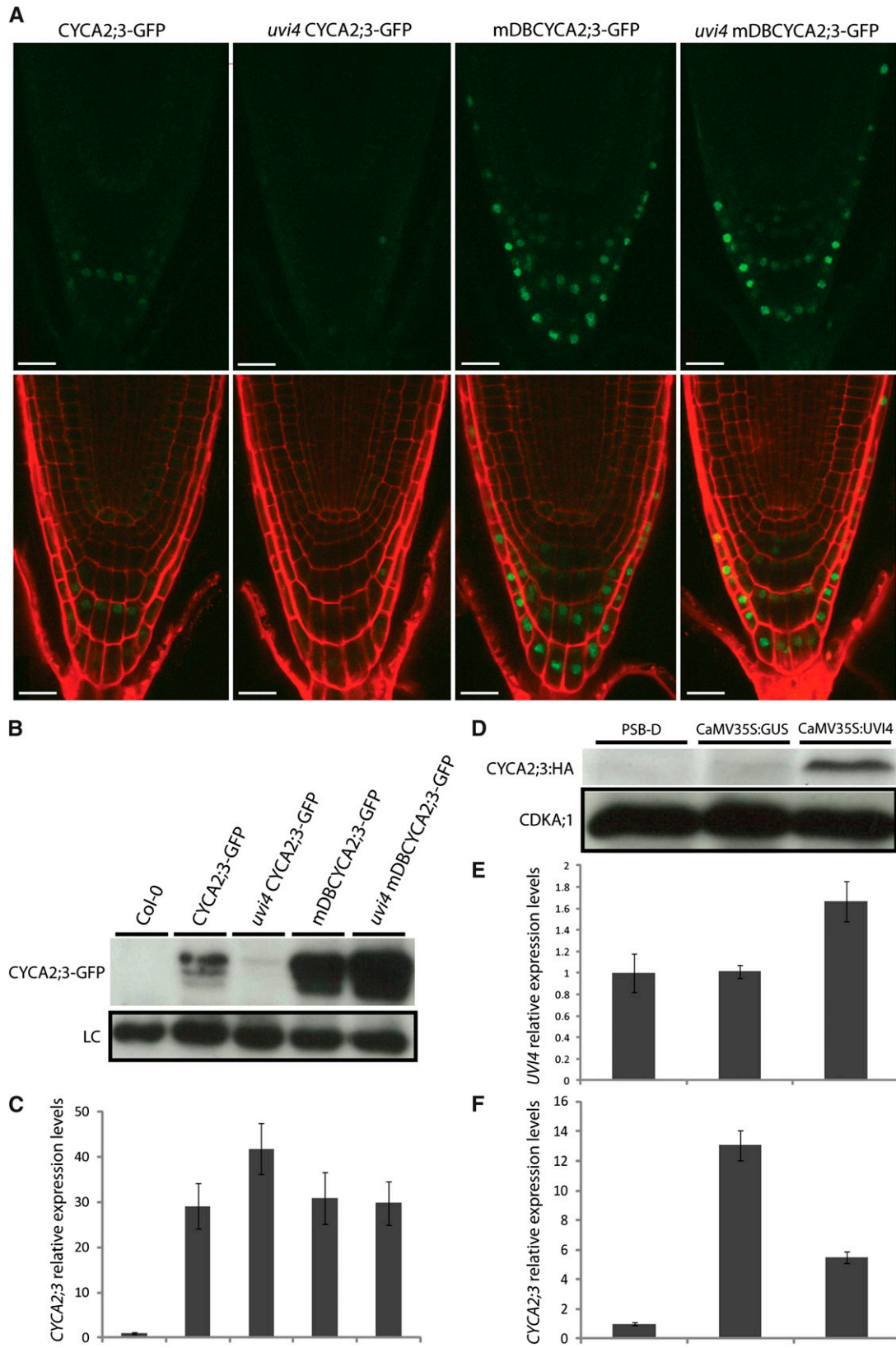
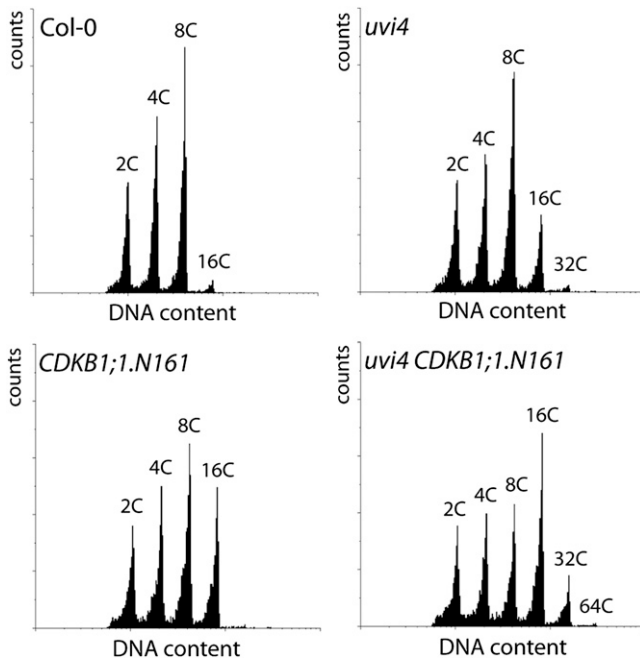**Figure 4.** Control of CYCA2;3 Abundance by UVI4.

Figure 5. Synergistic Regulation of Endocycle Onset by UVI4 and CDKB1;1.

Flow cytometric analysis of wild-type (Col-0), *uvi4*, *CDKB1;1.N161*, and *uvi4 CDKB1;1.N161* 3-week-old first leaves. Data represent mean $\pm$ SD (n = 3).

indirectly regulated E2F target genes (Berckmans and De Veylder, 2009). We tested whether *UVI4* expression is regulated by E2F transcription factors, despite the apparent lack of a consensus E2F binding cis-acting element in its promoter. *UVI4* transcript levels were found to increase 1.2-fold in *E2Fa*-overexpressing plants, and up to 4.9-fold after co-overexpression with its dimerization partner *DPa* (Figure 8C). By contrast, when *UVI4* transcript levels were assessed in *e2fa-2* loss-of-function mutants, no significant decrease could be observed. In *e2fb-1* loss-of-function plants, a decrease in *UVI4* expression levels of only 0.24-fold was observed, in contrast with the 0.54-fold reduction observed in an *e2fa-2 e2fb-1* double mutant, indicating that both E2Fa and E2Fb regulate *UVI4* expression (Figure 8D). To confirm this hypothesis, we performed a chromatin immunoprecipitation (ChIP) assay to analyze whether these transcription factors bind the *UVI4* promoter. *ETG1*, which has been shown previously to

be a target of both E2Fa and E2Fb, was included as a positive control, and actin as a negative control (Takahashi et al., 2008). After precipitation using the anti-E2Fa and anti-E2Fb antibodies, an enrichment of both the *ETG1* and *UVI4* promoters could be observed compared with the actin-negative control (Figures 8E and 8F). Together, these data show that both E2Fa and E2Fb transcription factors can bind to the *UVI4* promoter and regulate its expression.

UVI4 Allows CYCA2;3 Accumulation during the S Phase

The induction of *UVI4* transcripts at the G1-to-S transition and the control of CYCA2;3 abundance by UVI4 prompted us to investigate whether UVI4 might play a role in the temporal accumulation pattern of CYCA2;3. To this end, root tips from *CYCA2;3-GFP*-inducible overexpression plants were synchronized on medium containing both HU and β-estradiol. After 4, 6, and 8 h of synchronization, corresponding to maximum *UVI4* transcript levels, root tips were harvested from plants harboring CYCA2;3-GFP either in a wild-type or *uvi4* mutant background. CYCA2;3-GFP accumulation stabilized after 4 h of HU treatment in wild-type root tips and decreased after 6 h and 8 h of synchronization, but remained higher than initial levels. By contrast, in the *uvi4* mutant background, only a minor accumulation of CYCA2;3-GFP could be detected after 4 h (Figure 9). These data indicate that plants lacking UVI4 fail to accumulate CYCA2;3-GFP during DNA replication.

DISCUSSION

UVI4 Modulates Meristem Size by Regulating the Abundance of CYCA2;3

Here, we identified UVI4 as a negative regulator of APC/C^{CCS52A1} activity. By using the Y2H approach, we confirmed the previously reported TAP interaction between UVI4 and CCS52A1, but not with other APC/C subunits, including APC2, HBT, APC7, APC8, APC10, CDC20-1, and CCS52B (Van Leene et al., 2010). Failure to detect these interactions might be caused by the cooperative binding of UVI4 to different APC/C subunits. Nevertheless, CCS52A1 seems to be one of the most important APC/C contact sites, because the *uvi4* mutant trichome and leaf phenotypes were absent or strongly attenuated in *ccs52a1-1* knockout lines, which indicates that CCS52A1 is essential for UVI4 action. In leaf

---

Figure 4. (continued).

(A) Confocal images of induced *CYCA2;3-GFP* and D-box-mutated *mDBCYCA2;3-GFP* in wild-type or *uvi4* mutant root meristems. The top row of images shows the CYCA2;3-GFP signal, and the bottom row shows the CYCA2;3-GFP signal in combination with propidium iodide (PI) staining.
(B) Protein gel blot analysis with an anti-GFP antibody. LC, loading control corresponding to a nonspecific cross-reacting protein.
(C) Relative *CYCA2;3* expression levels of the lines presented in **(B)**. Expression levels in the wild type (Col-0) were arbitrarily set to one. Data represent mean $\pm$ SE (n = 3).
(D) CYCA2;3-HA protein levels in control (PSB-D), control transformed (*ROLD:CYCA2;3* and *CaMV35S:GUS*), and *UVI4*-overexpressing (*ROLD:CYCA2;3* and *CaMV35S:UVI4*) cell cultures. CDKA;1 proteins levels serve as loading control.
(E) and **(F)** Relative *UVI4* **(E)** and *CYCA2;3* **(F)** expression levels of the lines presented in **(D)**. Expression levels in wild type (PSB-D) were arbitrarily set to one. Data represent mean $\pm$ SE (n = 3).
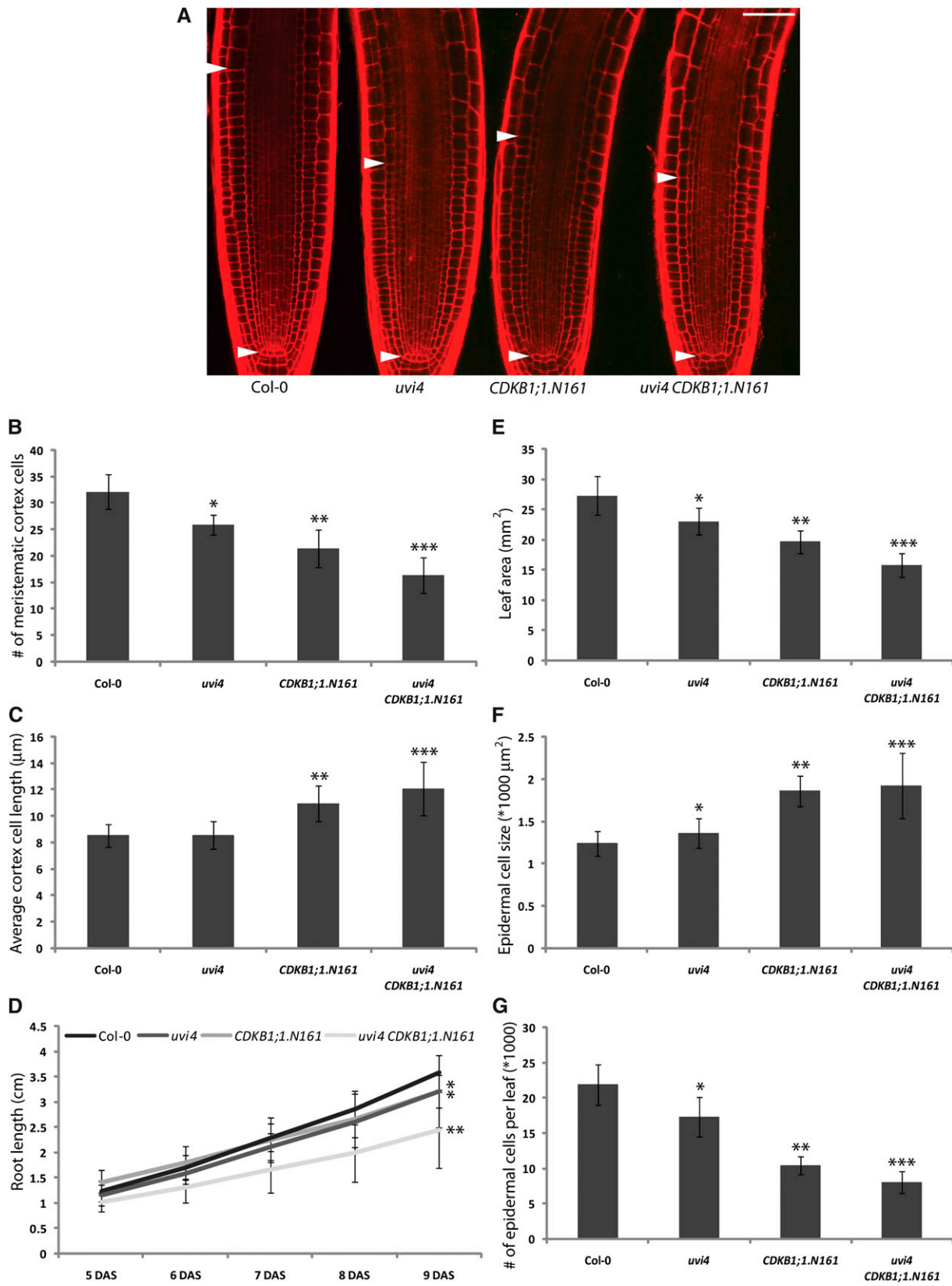Bars in **(A)** = 20 μm.

Figure 6. UVI4 Regulates Root Meristem Size.

tissues, the endoreduplication phenotype of *uvi4* was not completely repressed by the *ccs52a1-1* mutation. Because both CCS52A1 and CCS52A2 regulate endoreduplication in leaves (Lammens et al., 2008), UVI4 likely targets both CCS52A proteins for inhibition. Accordingly, although UVI4 interacted only with CCS52A1 in the Y2H screen, both CCS52A proteins copurified with UVI4 by TAP, suggesting that UVI4 also regulates APC/$C^{CCS52A2}$. However, protein immunoblots revealed that UVI4 preferentially interacted with CCS52A1 (see Supplemental Figure 4 online), at least in *Arabidopsis* cell cultures. Previously, we demonstrated that *CCS52A2* is regulated at the transcriptional level by the E2F/DP-E2F-Like1 (DEL1) transcription factor (Lammens et al., 2008). These data hint at the possibility that APC/$C^{CCS52A2}$ activity is regulated at two different levels: transcriptionally via DEL1 and posttranscriptionally by UVI4. Because the expression of both *DEL1* and *UVI4* is dependent on the phase of the cell cycle (see below), the combination of both mechanisms might fine-tune the timing of APC/C activity.

Arabidopsis encodes three E2F transcription factors, two transcriptional activators (E2Fa and E2Fb) and one repressor (E2Fc) (Berckmans and De Veylder, 2009). Analyses of *e2f* mutants and ChIP revealed that both the E2Fa and E2Fb transcription factors regulate *UVI4* expression, and this is probably the reason why transcript levels peak during the S phase. Although no consensus E2F binding motifs are present within 1000 nucleotides upstream of the *UVI4* start codon with the sequence matrix WTTSSCSS (where W = A or T, and S = C of G) that matches the most common E2F binding sites (Vandepoele et al., 2005), the *UVI4* promoter harbors two closely related sequences (see Supplemental Figure 5A online). A ChIP promoter scanning experiment revealed enrichment for E2Fa binding around these binding sites, suggesting that the putative E2F cis-regulatory elements represent functional ones (see Supplemental Figure 5B online).

Cell cycle phase-dependent expression of *UVI4* suggests that its gene product might play a role in the temporal control of APC/$C^{CCS52A1}$ activity. Previously, we have identified the S phase-specific cyclin CYCA2;3 as one of the critical substrates of the

APC/$C^{CCS52A1}$ regulating endocycle onset, as illustrated by the CYCA2;3-GFP protein stabilization in the root elongation zone in a *ccs52a1-1* mutant background (Boudolf et al., 2009), corresponding with the spatial expression pattern of *CCS52A1* (Vanstraelen et al., 2009). Here, we showed that CYCA2;3 destruction through the APC/C is regulated by UVI4. Knockout plants for *UVI4* display reduced CYCA2;3 levels, whereas overexpression of *UVI4* results in cyclin stabilization. When comparing synchronized root tips of wild-type and *uvi4* mutant plants, the UVI4 activity was found to be required for the accumulation of CYCA2;3 during the S phase progression. We hypothesize that this accumulation is a prerequisite for cells to progress through the G2-to-M transition (Figure 10A). CYCA2;3-regulated CDK activity might be needed to activate the three-repeat MYB transcription factors that regulate the expression of G2/M-expressed genes (Ito et al., 2001). In the absence of UVI4, cells can finalize the DNA replication but not enter into a mitotic event, eventually entering an endocycle instead, with polyploidy as a consequence (Figure 10B). Nevertheless, despite the smaller root meristem size, mitotic divisions are not totally suppressed in *UVI4*-deficient roots, suggesting that redundant mechanisms regulate CYCA2;3 abundance. In the young meristematic cells, strong *CYCA2;3* transcription or CCS52A inactivation through CDK phosphorylation might represent alternative mechanisms to inhibit APC/C activity, allowing CYCA2;3 to accumulate. As cells age, the importance of these alternative mechanisms might decrease, at which point UVI4 action might become the most important factor to regulate CYCA2;3 abundance.

By mediating mitotic entry, UVI4 indirectly regulates the meristem size and the plant growth rate. CYCA2;3 has previously been found to be an important factor in the suppression of cell cycle exit. Ectopic accumulation of the CYCA2;3-GFP fusion protein activates cell proliferation, whereas the loss of function mutation stimulates cell cycle exit and onset of endoreduplication (Imai et al., 2006). CYCA2;3 forms a functional complex with CDKB1;1 (Boudolf et al., 2009), of which the kinase activity is essential in the maintenance of cell division (Boudolf et al., 2004). Together with the meristematic expression pattern of *UVI4* (Hase

---

Figure 6. (continued).

(A) Representative confocal microscopy images of wild-type (Col-0), *uvi4*, *CDKB1;1.N161*, and *uvi4 CDKB1;1.N161* 1-week-old root meristems stained with PI. Arrowheads indicate the meristem size based on the cortical cell length.

(B) and **(C)** Number of meristematic cortex cells **(B)** and their average cell length **(C)** for lines presented in **(A)**. Data represent mean ± SD ($n > 12$). The *uvi4* mutant has a significant decrease in the number of meristematic cortex cells compared with the wild type (Col-0) (*P value < 0.05, Student's *t* test). The *CDKB1;1.N161* mutant has a significant decrease in the number of meristematic cortex cells and an increase in their average cell length compared with the *uvi4* mutant (**P value < 0.05, Student's *t* test). The *uvi4 CDKB1;1.N161* double mutant has a significant decrease in the number of meristematic cortex cells and an increase in their average cell length compared with both *uvi4* and *CDKB1;1.N161* single mutants (***P value < 0.05, Student's *t* test).

(D) Root length of lines presented in **(A)** plotted from 5 to 9 d after sowing. Data represent mean ± SD ($n > 27$). Both *uvi4* and *CDKB1;1.N161* mutants have a significantly decreased root length compared with the wild type (Col-0) (*P value < 0.05, Student's *t* test). The *uvi4 CDKB1;1.N161* double mutant has a significantly decreased root growth compared with both *uvi4* and *CDKB1;1.N161* single mutants (**P value < 0.05, Student's *t* test).

(E) to **(G)** Leaf size **(E)**, average abaxial epidermal cell size **(F)**, and cell number **(G)** of 3-week-old first leaves of the lines presented in **(A)**. Data represent mean ± SD ($n \geq 9$). The *uvi4* mutant has a significant decrease in leaf size and cell number and an increased average abaxial epidermal cell size compared with the wild type (Col-0) (*P value < 0.05, Student's *t* test). The *CDKB1;1.N161* mutant has a significant decrease in leaf size and cell number and an increased average abaxial epidermal cell size compared with the *uvi4* mutant (**P value < 0.05, Student's *t* test). The *uvi4 CDKB1;1.N161* double mutant has a significant decrease in leaf size and cell number, an increased average abaxial epidermal cell size compared with the *uvi4* single mutant, and a significant decrease in leaf size and cell number compared with the *CDKB1;1.N161* single mutant (***P value < 0.05, Student's *t* test).

Bars in **(A)** =50 µm.
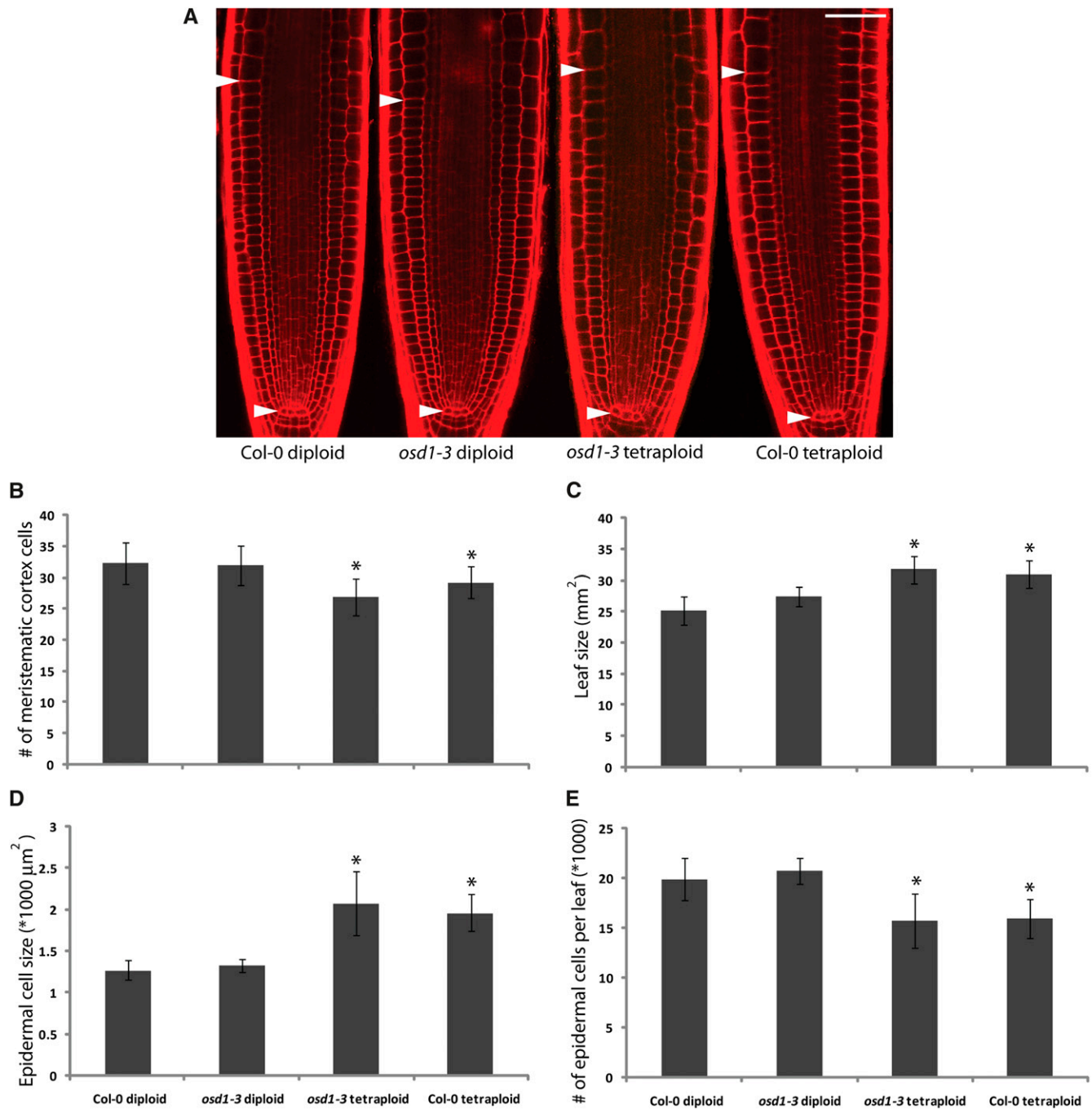
[See online article for color version of this figure.]

Figure 7. OSD1 Does Not Regulate Meristem Size.

(A) Representative confocal microscopy images of wild-type (Col-0), *osd1-3* diploid, *osd1-3* tetraploid, and Col-0 tetraploid 1-week-old root meristems stained with PI. Arrowheads indicate the total meristem length based on the cortical cell length.

(B) Number of meristematic root cortex cells in control (Col-0), *osd1-3* diploid, *osd1-3* tetraploid, and Col-0 tetraploid plants. Data represent mean ± SD (*n* ≥ 19). The *osd1-3* diploid mutant shows no significant difference compared with wild-type (Col-0) but has a significant increase in cortex cell number compared with the *osd1-3* tetraploid mutant and Col-0 tetraploid plants (*P value < 0.05, Student's *t* test). The *osd1-3* tetraploid mutant shows no significant difference with Col-0 tetraploid plants.

(C) to **(E)** Leaf size **(C)**, average abaxial epidermal cell size **(D)**, and cell number **(E)** of 3-week-old first leaves of lines presented in **(A)**. Data represent mean ± SD (*n* ≥ 7).The *osd1-3* diploid mutant shows no significant difference compared with the wild type (Col-0) but has a significantly decreased leaf size and an average abaxial epidermal cell size and cell number compared with the *osd1-3* tetraploid mutant and Col-0 tetraploid plants (*P value < 0.05). The *osd1-3* tetraploid mutant shows no significant difference with Col-0 tetraploid plants.

Bars in **(A)** = 50 μm.
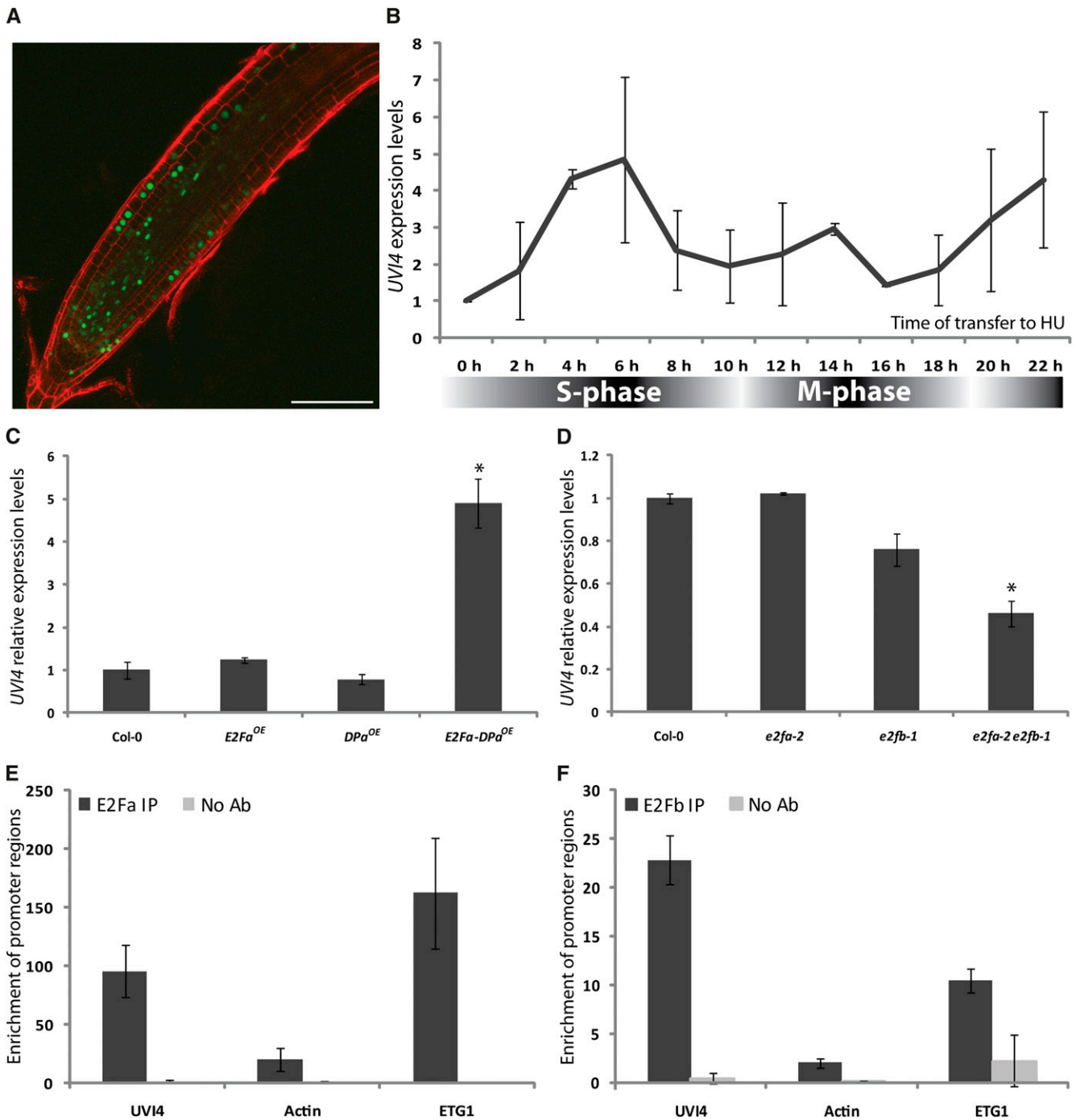
[See online article for color version of this figure.]

Figure 8. Expression of *UVI4* Is Cell Cycle Phase Dependently Regulated by E2F Transcription Factors.

(A) Confocal microscopy image of a *UVI4:UVI4-GFP* root tip counterstained with PI. The patchy nuclear GFP signal suggests a cell cycle phase-specific expression.
(B) Relative *UVI4* expression levels in HU-synchronized root tips. The transcript level of nonsynchronized root tips (0 h) was arbitrarily set to 1. Data represent mean ± SE ($n = 2$).
(C) and **(D)** Relative *UVI4* expression levels in control (Col-0), *E2Fa*, *DPa*, and *E2Fa-DPa* overexpression plants **(C)** and *e2fa-2*, *e2fb-1*, and *e2fa-2 e2fb-1* mutants **(D)**. The transcript level of Col-0 was arbitrarily set to 1. Data represent mean ± SE (*P value < 0.05, Student's *t* test, $n = 3$).
(E) and **(F)** Promoter element enrichments after ChIP from 1-week-old *Arabidopsis* seedlings with the E2Fa **(E)** and E2Fb **(F)** antibodies and with actin and *ETG1* as a negative and positive control, respectively. For E2Fa, the no-antibody control values were extremely low compared with those of the E2Fa antibody and IP and were hence not visible on the graph. Data represent mean ± SE ($n = 2$).
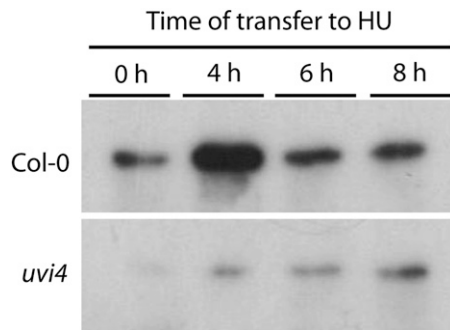Bar in **(A)** = 100 μm.

Time of transfer to HU

	0 h	4 h	6 h	8 h

Col-0

uvi4

Figure 9. UVI4 Regulates CYCA2;3 Accumulation during the S Phase.

CYCA2;3-GFP levels in wild-type (Col-0) and *uvi4* HU-synchronized root tips measured by protein gel blotting with an anti-GFP antibody.

et al., 2006), this suggests that UVI4 might allow the accumulation of CYCA2;3-CDKB1;1 activity in dividing cells, in that way negating the possible premature action of CCS52A1, and thus preventing premature cell cycle exit. In agreement with this hypothesis, *uvi4* mutant plants display a reduced growth and meristem size. This effect is even more pronounced in a *CDKB1;1.N161* overexpression background, probably because of an even stronger decrease in CYCA2;3 levels.

UVI4, a Functional Homolog of Emi1

UVI4 shares structural and functional features with animal APC/C inhibitors, such as Emi1. From both our protein interaction

studies and genetic complementation tests with *uvi4* mutant alleles, we conclude that the deletion of the conserved MR tail results in the loss of the APC/C interaction and UVI4 function. Likewise, the C-terminal RL tail in the Emi1 and Emi2/Erp1 sequence has been shown to be essential for the APC/C inhibitory activity (Miller et al., 2006). However, there are also structural differences. Besides the RL tail, detailed studies of the Emi1- and Erp1/Emi2-conserved D-boxes have revealed that this degron is needed for APC/C interaction as well, because its mutation reduces APC/C binding and activity (Miller et al., 2006; Ohe et al., 2010). By contrast, the D-box motif is seemingly not essential for UVI4 activity in *Arabidopsis*; however, its mutation abrogates the interaction with CCS52A1 in the Y2H system. Inhibitory activity of the D-box mutant can be explained by the cooperative binding of UVI4 to the APC/C holocomplex in vivo. The D-box might contribute to the CCS52A1 interaction, as suggested by the Y2H experiment, but interactions using the GxEN motif and MR tail might be sufficient to achieve APC/C inhibition. Thus, our results suggest that, as observed for Emi1 and Erp1/Emi2, the D-box might interact directly with CCS52A1, whereas the MR tail, together with the GxEN motif, might mediate the interaction of UVI4 with the APC/C holocomplex.

At the functional level, just like UVI4, the mammalian Emi1 is needed for cells to enter mitosis. *Xenopus* extracts depleted of Emi1 do not enter mitosis, because they cannot accumulate cyclin B (Reimann et al. 2001). Likewise, depletion of Emi1 in mammalian cells induces DNA re-replication, because APC/C^{CDH1} cannot be turned off, resulting in the continuous degradation of several APC/C substrates, including cyclin A (Di Fiore and Pines 2007; Machida and Dutta 2007). Moreover, as
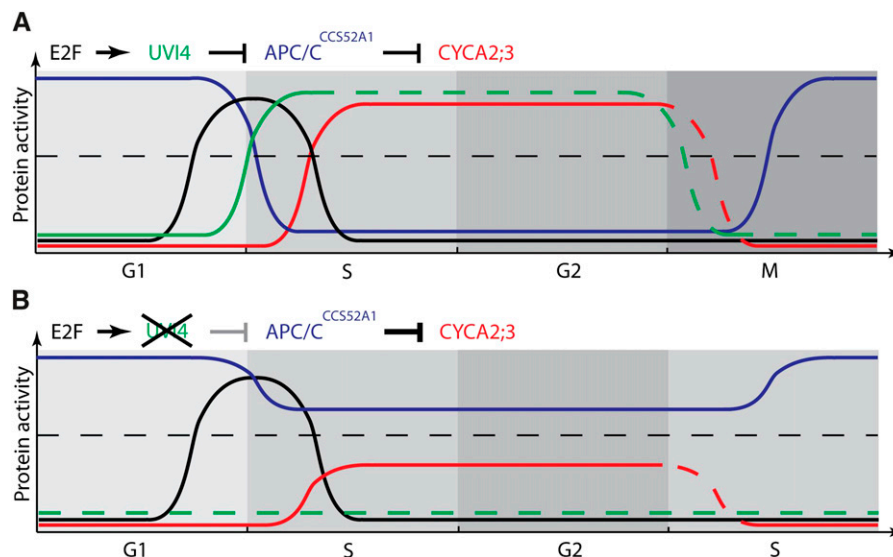
Figure 10. Model for UVI4 Action.

In wild-type plants, UVI4 levels increase at the G1-to-S transition because of the E2F activity. UVI4 inhibits APC/$C^{CCS52A1}$ activity and allows the increase of CYCA2;3 levels and the occurrence of the G2-to-M transition **(A)**. In the absence of UVI4, the APC/$C^{CCS52A1}$ activity probably drops only marginally, possibly through the negative regulation by CDK phosphorylation that allows a partial, but insufficient, increase in the CYCA2;3 abundance to trigger the G2-to-M transition, with endoreduplication as a consequence **(B)**. The dashed black horizontal line represents a hypothetical CYCA2;3 accumulation threshold needed to proceed into mitosis. Full and dashed colored lines represent experimentally demonstrated and speculated activities derived from homology with other eukaryotic systems, respectively.

observed in *Arabidopsis*, phenotypes of *Emi1* mutant cells can be suppressed by mutations in *CDH1*. Finally, both UVI4 and Emi1 seem to be required for the repression of APC/C activity during the S-to-G2 transition, coupling DNA replication with mitosis, whereby the E2F transcription factors seemingly regulate the timing of activity of both genes (Hsu et al., 2002).

UVI4 and Emi1 are not only structurally and functionally related, but also both possess a homolog that operates specifically in the meiotic cell cycle, namely OSD1 and Erp1/Emi2, respectively (Tung et al., 2005; Ohe et al., 2007; d'Erfurth et al., 2009), that are both essential for the transition from meiosis I to meiosis II (Ohe et al., 2007; d'Erfurth et al., 2010). In *Xenopus*, this transition occurs through a stabilization of CYCB by Erp1/Emi2 (Ohe et al., 2007), whereas the targets of OSD1 remain to be identified. Taken together, we postulate that UVI4 and OSD1 correspond to functional homologs of Emi1 and Erp1/Emi2 that encode APC/C inhibitors, which play an important role in sustaining the mitotic and meiotic cell cycle, respectively. The Emi1 and Erp1/Emi2 APC/C inhibitors have been shown to operate by acting as pseudosubstrates by D-box recognition and by blocking the catalytic cleft by means of their conserved C-terminal zinc-binding region (Miller et al., 2006). Although no zinc binding or other putative APC/C inhibitory domains occurred in the sequence alignment of UVI4, we cannot exclude the possibility that an unidentified plant-specific domain also exerts the inhibitory function. Further functional mapping and three-dimensional structure information on UVI4 can shed light on how UVI4 plays its role as APC/C inhibitor.

METHODS

Antibody Generation

An anti-UVI4 antibody was raised against the N-terminally located GQIQFRSPQGRENMSLG(C) (83 to 99) peptide in rabbits. The C-terminal Cys was added to allow KLH coupling of the peptide. Peptides were synthesized and rabbits immunized by Agro-Bio.

Gene Constructs and Site-Specific Mutagenesis

The full-length cDNA of *UVI4* was cloned, and the D1, D2, and G degrons were mutated with a two-step adaptor ligation PCR approach. Adaptor primers containing the mutated sequence were used to amplify the open reading frame (ORF) 5′ and 3′ of the respective site. Ligation of the two fragments was achieved in a second PCR step. The UVI4 −MR mutant was designed by deletion of the six corresponding 3′ terminal nucleotides. The *UVI4* alleles were inserted into the pK7m24GW plasmid under control of the *UVI4* promoter, the region of 1046 nucleotides upstream of the start codon. The GFP-UVI4 fusion construct was generated by recombining *UVI4* and *GFP* into the pH7m34GW plasmid, under control of the *UVI4* promoter. The PCR primer sequences used for cloning are given in Supplemental Table 3 online. Constructs were generated by Gateway cloning (Invitrogen).

Plant Medium and Growth Conditions

Plants were grown under a long-day/short-night regime (16 h light/8 h darkness) at 21°C on agar-solidified culture medium [Murashige and Skoog (MS) medium, 10 g/L saccharose, 0.43 g/L 2-(N-morpholino)-ethane-sulfonic acid, and 0.8% plant tissue culture agar]. *UVI4* comple-

mentation plants were screened using 45 mg/L kanamycin selection; plants harboring the *GFP-UVI4* fusion construct were selected using 15 mg/L hygromycin. The root meristem was synchronized as described (Cools et al., 2010). For *CYCA2;3-GFP* induction, plants were grown on vertical MS medium for 5 d and then transferred with nylon meshes (Prosep) to MS medium containing 10 µM β-estradiol (Sigma-Aldrich) for an additional 2 d. For synchronization of *CYCA2;3-GFP* plants, 2 d after induction, seedlings were transferred to MS plates containing both 10 µM β-estradiol and 2 mM HU (Sigma-Aldrich).

Arabidopsis Cell Suspension Culture Transformation and Cultivation

The *UVI4* and *CYCA2;3-HA* ORF were inserted into the pK7m34GW2-8m21GW3D vector, under control of the *CaMV35S* and *ROLD* constitutive promoters, respectively, through recombination using the Gateway LR II Plus enzyme mix. As a control, the *GUS*-encoding gene was recombined instead of the *UVI4* ORF. Transformation and cultivation of *Arabidopsis thaliana* cell suspension cultures was performed as previously described by Van Leene et al. (2007).

Mutant Lines

The *osd1-3* transfer DNA (T-DNA) insertion mutant was obtained from the Koncz collection in Cologne. The T-DNA was inserted 58 nucleotides after the start codon of the second exon, resulting in the removal of the last 109 amino acids of the 243-amino-acid-long OSD1 (see Supplemental Figure 6 online). Primers used for genotyping are given in Supplemental Table 3 online. The *ccs52a1-1*, *ccs52a2-1* (Lammens et al., 2008), *CDKB1;1.N161* (Boudolf et al., 2004), *e2fa-2* and *e2fb*-1 (Berckmans et al., 2011b), inducible *CYCA2;3-GFP* and *mDBCYCA2;3-GFP* (Imai et al., 2006), and tetraploid Col-0 (Tsukaya, 2008) lines had been described previously. The *uvi4* mutant was obtained from Yoshihiro Hase (RIKEN Institute, Yokohama, Japan). Double mutants were generated by crossing.

Y2H Interactions

Plasmids encoding the bait (pDEST32) and prey (pDEST22) were transformed into the yeast strain PJ69-4α (MATα; trp1-901, leu2-3,112, ura3-52, his3-200, gal4Δ, gal80Δ, LYS2::GAL1-HIS3, GAL2-ADE2, met2GAL7-lacZ) and PJ69-4a (MATa; trp1-901, leu2-3,112, ura3-52, his3-200, gal4Δ, gal80Δ, LYS2TGAL1-HIS3, GAL2-ADE2, met2TGAL7-lacZ) by the LiAc method (Gietz et al., 1992). Transformed yeast cells were selected on synthetic dextrose plates without Leu (pDEST 32) or without Trp (pDEST22). Interactions between proteins were assayed by the mating method. All pDEST32 yeast cultures were inoculated in 200 µL synthetic dextrose without Trp in a 96-well microtiter plate (Falcon; BD Biosciences), whereas one pDEST22 yeast culture was inoculated in 50 mL synthetic dextrose medium without Leu. To scale up the yeast cultures, 20 µL of each culture grown for 2 d at 30°C was added to a microtiter plate containing 125 µL of Glc-containing rich medium (10 g/L bacto-yeast extract, 10 g/L bacto-peptone, and 20% dextrose) and again grown for 24 h at 30°C. The Glc-containing rich medium was replaced by synthetic dextrose medium without Leu and Trp. Diploid strains grown in a 96-well microtiter plate (NUNC) for 2 d at 30°C were diluted until $OD_{600} = 0.2$ and then added to a 96-well microtiter plate (Falcon; BD Biosciences) containing either 190 µL synthetic dextrose medium without Leu and Trp but with His (as control), or synthetic dextrose medium without Leu, Trp, or His. The OD was measured after 2 d of incubation at 30°C. Interactions were scored positive when the ratio of the OD_{600} of the synthetic dextrose medium without Leu, Trp, or His or that of the synthetic dextrose medium without Leu and Trp exceeded the threefold average background value of the negative controls.

Protein Extraction and Purification

Whole plant tissue and cell suspension cultures were ground with 4-mm metal beads, and proteins were extracted with homogenization buffer (Boudolf et al., 2009). CYCA2;3-GFP was purified with the agarose-conjugated anti-GFP from MBL (D153-8) by incubating the agarose beads with 100 μg of total protein extract for 1 h at 4°C. After three washes with cold lysis buffer (Boudolf et al., 2009), beads were boiled in 5× sample buffer (350 mM Tris-HCL, pH 6.8, 10% SDS, 600 mM dithiothreitol, 0.012% bromophenol blue, 30% glycerol), and the supernatant was separated by SDS-PAGE. After protein immunoblotting, CYCA2;3-GFP was visualized with the Living Colors Monoclonal Antibody (JL-8) (Clontech). For the inducible *CYCA2;3-GFP* and *UVI4-GFP* root synchronization experiments, 35 μg and 250 μg total protein extract were incubated with anti-GFP agarose for 1 h at 4°C, respectively. Total cell suspension protein extract was made using the same method, and 300 μg was separated by SDS-PAGE. CYCA2;3-HA was visualized after protein gel blotting with the Anti-HA High-Affinity Rat monoclonal antibody (clone 3F10) (Roche).

ChIP

ChIP was performed with the anti-E2Fa and anti-E2Fb antibodies according to the protocol of Berckmans et al. (2011a). As a negative control, immunoprecipitation was performed without any antibody. The promoter-scanning ChIP experiment was performed using a *Pro35S*: *E2Fa*-overexpressing *Arabidopsis* cell suspension culture. Maintenance and stable transformation of *Arabidopsis* PSB-D cell suspension cultures was done according to Van Leene et al. (2007). qPCR experiments were performed on equal concentrations of total, mock ChIP, and E2Fa ChIP DNA, as measured with the Quant-iT dsDNA High Sensitivity Kit (Invitrogen). Primers used for PCR amplification were designed to span the complete upstream region of *UVI4*, up to the next gene, using Primer-BLAST (http://www.ncbi.nlm.nih.gov/tools/primer-blast/). PCR primer sequences are given in Supplemental Table 3 online. Normalization of enrichment relative to total input DNA was calculated as $2^{(Ct(input) - Ct(purified))}$.

Confocal and Scanning Electron Microscopy

Root meristems were analyzed using a Zeiss Axiovert 100M confocal laser scanning microscope. Plant material was incubated for 2 min in a 10-μm PI solution to stain the cell walls and was observed under an epifluorescence light with the appropriate filter set (excitation filter, 535 to 550 nm; dichroic mirror, 565 nm; barrier filter, 590 nm). GFP fluorescence was detected with a 500- to 550-nm band-pass emission filter. Images of leaf trichomes were acquired with a TM-1000 Tabletop electron microscope (Hitachi).

Quantification of Trichome Nuclear DNA Content

For DAPI staining, 3-week-old mature leaves were fixed using acetic acid (75% acetic acid, 25% ethanol) for 2 h and washed for 1 h with 70% ethanol. Leaves were briefly submerged in EDTA (0.5 M), and trichomes were removed using forceps. DNA was stained using 20 μg/mL DAPI in McIlvaine's buffer (60 mM citric acid, 80 mM Na_2HPO_4, pH 4.1). Trichomes were mounted in Vectashield mounting medium for fluorescence H1000 (Vector laboratories; no. CA94010) and observed via epifluorescence on an Axioscope Imager microscope from Zeiss. Nuclear size and epifluorescence signal were analyzed using the ImageJ 1.41 software. The integrated density was calculated by multiplication of nuclear size and fluorescence intensity, normalized against the integrated density of wild-type Col-0 trichome nuclei. Wild-type trichome nuclear size was arbitrarily set to 32C.

RT-qPCR Analysis

RNA was extracted from the respective tissues with the RNeasy Kit (Qiagen). After DNase treatment with the RQ1 RNase-Free DNase (Promega), cDNA was synthesized with the iScript cDNA Synthesis Kit (Bio-Rad). Relative expression levels were determined with the Light-Cycler 480 Real-Time SYBR green PCR System (Roche). Two different reference genes were used for normalization, depending on the source of the tissue. ACT (At3G18780) and UBQ10 (At4G05320) were used for cell suspension cultures, ACT and CKII (At3G50000) for plant material, and PAC1 (At3G22110) and EMB2386 (At1G02780) for root tip synchronization. Primer sequences used for RT-qPCR analyses are given in Supplemental Table 3 online.

Flow Cytometry

Leaves were chopped with a razor blade in 200 μL CyStain UV Precise nuclei extraction buffer (Partec), and DNA was stained by adding 800 μL staining buffer (Partec). Nuclei were measured with a CyFlow Flow Cytometer (Partec) and analyzed with the FloMax software (Partec). Unless stated otherwise, three or more leaves were analyzed for each technical repeat.

Accession Numbers

Sequence data from this article can be found in the Arabidopsis Genome Initiative or GenBank/EMBL databases under the following accession numbers: *UVI4* (At2G42260); *OSD1* (At3G57860); *CCS52A1* (At4G29910); CYCA2;3 (At1g15570); *CDKB1;1* (At3G54180); *E2Fa* (At2G36010); *E2Fb* (At5G22220); *DPa* (At5G02470).

Supplemental Data

The following materials are available in the online version of this article.

Supplemental Figure 1. Quantification of the Wild-Type (Col-0) and *uvi4*, *ccs52a1-1*, and *uvi4 ccs52a1-1* Mutant Trichome Branch Number.

Supplemental Figure 2. Quantification of Nuclear DNA Content of the Wild-Type (Col-0) and *uvi4*, *ccs52a1-1*, and *uvi4 ccs52a1-1* Mutant Trichomes.

Supplemental Figure 3. Cell Cycle Phase-Dependent Accumulation of the UVI4-GFP Protein.

Supplemental Figure 4. Copurification of UVI4 with CCS52A1 and CCS52A2.

Supplemental Figure 5. Binding of E2Fa to the *UVI4* Promoter.

Supplemental Figure 6. Graphical Representation of the T-DNA Insertion in the *osd1-3* Line.

Supplemental Table 1. Ploidy Distribution of 3-Week-Old First Leaves of the Wild Type (Col-0) and the *uvi4*, *ccs52a1-1*, and *uvi4 ccs52a1-1* Mutants.

Supplemental Table 2. Ploidy Distribution of 3-Week-Old First Leaves of the Wild Type (Col-0) and the *uvi4*, *CDKB1;1.N161*, and *uvi4 CDKB1;1.N161* Mutants.

Supplemental Table 3. Primer Sequences Used for Cloning, Genotyping, RT-qPCR, and ChIP Analysis.

Supplemental Data Set 1. Pairwise Y2H Interactions Tested between *Arabidopsis* APC/C Proteins.

AUTHOR CONTRIBUTIONS

J.H., C.K., G.D.J., and L.D.V. conceived and designed the experiments. J.H., H.V.D.D., K.D.W; V.B., B.B., A.V., and C.L.A.K performed the experiments. J.H. and L.D.V. analyzed the data. J.H. and L.D.V. wrote the article.

REFERENCES

Beemster, G.T.S., De Veylder, L., Vercruysse, S., West, G., Rombaut, D., Van Hummelen, P., Galichet, A., Gruissem, W., Inzé, D., and Vuylsteke, M. (2005). Genome-wide analysis of gene expression profiles associated with cell cycle transitions in growing organs of Arabidopsis. Plant Physiol. **138:** 734–743.

Berckmans, B., and De Veylder, L. (2009). Transcriptional control of the cell cycle. Curr. Opin. Plant Biol. **12:** 599–605.

Berckmans, B., Lammens, T., Van Den Daele, H., Magyar, Z., Bögre, L., and De Veylder, L. (2011a). Light-dependent regulation of *DEL1* is determined by the antagonistic action of E2Fb and E2Fc. Plant Physiol. **157:** 1440–1451.

Berckmans, B., et al. (2011b). Auxin-dependent cell cycle reactivation through transcriptional regulation of *Arabidopsis E2Fa* by lateral organ boundary proteins. Plant Cell **23:**. 3671–3683.

Boruc, J., Van den Daele, H., Hollunder, J., Rombauts, S., Mylle, E., Hilson, P., Inzé, D., De Veylder, L., and Russinova, E. (2010). Functional modules in the *Arabidopsis* core cell cycle binary protein-protein interaction network. Plant Cell **22:** 1264–1280.

Boudolf, V., Vlieghe, K., Beemster, G.T.S., Magyar, Z., Torres Acosta, J.A., Maes, S., Van Der Schueren, E., Inzé, D., and De Veylder, L. (2004). The plant-specific cyclin-dependent kinase CDKB1;1 and transcription factor E2Fa-DPa control the balance of mitotically dividing and endoreduplicating cells in *Arabidopsis*. Plant Cell **16:** 2683–2692.

Boudolf, V., et al. (2009). CDKB1;1 forms a functional complex with CYCA2;3 to suppress endocycle onset. Plant Physiol. **150:** 1482–1493.

Bramsiepe, J., Wester, K., Weinl, C., Roodbarkelari, F., Kasili, R., Larkin, J.C., Hülskamp, M., and Schnittger, A. (2010). Endoreplication controls cell fate maintenance. PLoS Genet. **6:** e1000996.

Bulankova, P., Riehs-Kearnan, N., Nowack, M.K., Schnittger, A., and Riha, K. (2010). Meiotic progression in *Arabidopsis* is governed by complex regulatory interactions between SMG7, TDM1, and the meiosis I-specific cyclin TAM. Plant Cell **22:** 3791–3803.

Burton, J.L., Xiong, Y., and Solomon, M.J. (2011). Mechanisms of pseudosubstrate inhibition of the anaphase promoting complex by Acm1. EMBO J. **30:** 1818–1829.

Capron, A., Serralbo, O., Fülöp, K., Frugier, F., Parmentier, Y., Dong, A., Lecureuil, A., Guerche, P., Kondorosi, E., Scheres, B., and Genschik, P. (2003). The *Arabidopsis* anaphase-promoting complex or cyclosome: molecular and genetic characterization of the APC2 subunit. Plant Cell **15:** 2370–2382.

Castro, A., Vigneron, S., Bernis, C., Labbé, J.-C., and Lorca, T. (2003). Xkid is degraded in a D-box, KEN-box, and A-box-independent pathway. Mol. Cell. Biol. **23:** 4126–4138.

Cebolla, A., Vinardell, J.M., Kiss, E., Oláh, B., Roudier, F., Kondorosi, A., and Kondorosi, E. (1999). The mitotic inhibitor *ccs52* is required for endoreduplication and ploidy-dependent cell enlargement in plants. EMBO J. **18:** 4476–4484.

Cools, T., Iantcheva, A., Maes, S., Van den Daele, H., and De Veylder, L. (2010). A replication stress-induced synchronization method for *Arabidopsis thaliana* root meristems. Plant J. **64:** 705–714.

d'Erfurth, I., Jolivet, S., Froger, N., Catrice, O., Novatchkova, M., and Mercier, R. (2009). Turning meiosis into mitosis. PLoS Biol. **7:** e1000124.

d'Erfurth, I., Cromer, L., Jolivet, S., Girard, C., Horlow, C., Sun, Y., To, J.P.C., Berchowitz, L.E., Copenhaver, G.P., and Mercier, R. (2010). The cyclin-A CYCA1;2/TAM is required for the meiosis I to meiosis II transition and cooperates with OSD1 for the prophase to first meiotic division transition. PLoS Genet. **6:** e1000989.

Di Fiore, B., and Pines, J. (2007). Emi1 is needed to couple DNA replication with mitosis but does not regulate activation of the mitotic APC/C. J. Cell Biol. **177:** 425–437.

Dolan, L., Janmaat, K., Willemsen, V., Linstead, P., Poethig, S., Roberts, K., and Scheres, B. (1993). Cellular organisation of the *Arabidopsis thaliana* root. Development **119:** 71–84.

Eloy, N.B., Coppens, F., Beemster, G.T.S., Hemerly, A.S., and Ferreira, P.C.G. (2006). The *Arabidopsis* anaphase promoting complex (APC): Regulation through subunit availability in plant tissues. Cell Cycle **5:** 1957–1965.

Gietz, D., St Jean, A., Woods, R.A., and Schiestl, R.H. (1992). Improved method for high efficiency transformation of intact yeast cells. Nucleic Acids Res. **20:** 1425.

Grosskortenhaus, R., and Sprenger, F. (2002). Rca1 inhibits APC-Cdh1(Fzr) and is required to prevent cyclin degradation in G2. Dev. Cell **2:** 29–40.

Hase, Y., Trung, K.H., Matsunaga, T., and Tanaka, A. (2006). A mutation in the *uvi4* gene promotes progression of endo-reduplication and confers increased tolerance towards ultraviolet B light. Plant J. **46:** 317–326.

Hershko, A. (1997). Roles of ubiquitin-mediated proteolysis in cell cycle control. Curr. Opin. Cell Biol. **9:** 788–799.

Hsu, J.Y., Reimann, J.D.R., Sørensen, C.S., Lukas, J., and Jackson, P.K. (2002). E2F-dependent accumulation of hEmi1 regulates S phase entry by inhibiting APC(Cdh1). Nat. Cell Biol. **4:** 358–366.

Imai, K.K., Ohashi, Y., Tsuge, T., Yoshizumi, T., Matsui, M., Oka, A., and Aoyama, T. (2006). The A-type cyclin CYCA2;3 is a key regulator of ploidy levels in *Arabidopsis* endoreduplication. Plant Cell **18:** 382–396.

Inzé, D., and De Veylder, L. (2006). Cell cycle regulation in plant development. Annu. Rev. Genet. **40:** 77–105.

Ito, M., Araki, S., Matsunaga, S., Itoh, T., Nishihama, R., Machida, Y., Doonan, J.H., and Watanabe, A. (2001). G2/M-phase-specific transcription during the plant cell cycle is mediated by c-Myb-like transcription factors. Plant Cell **13:** 1891–1905.

Kasili, R., Walker, J.D., Simmons, L.A., Zhou, J., De Veylder, L., and Larkin, J.C. (2010). SIAMESE cooperates with the CDH1-like protein CCS52A1 to establish endoreplication in *Arabidopsis thaliana* trichomes. Genetics **185:** 257–268.

Lammens, T., Boudolf, V., Kheibarshekan, L., Zalmas, L.P., Gaamouche, T., Maes, S., Vanstraelen, M., Kondorosi, E., La Thangue, N.B., Govaerts, W., Inzé, D., and De Veylder, L. (2008). Atypical E2F activity restrains APC/CCCS52A2 function obligatory for endocycle onset. Proc. Natl. Acad. Sci. USA **105:** 14721–14726.

Lénárt, P., and Peters, J.-M. (2006). Checkpoint activation: Don't get mad too much. Curr. Biol. **16:** R412–R414.

Machida, Y.J., and Dutta, A. (2007). The APC/C inhibitor, Emi1, is essential for prevention of rereplication. Genes Dev. **21:** 184–194.

Marrocco, K., Bergdoll, M., Achard, P., Criqui, M.-C., and Genschik, P. (2010). Selective proteolysis sets the tempo of the cell cycle. Curr. Opin. Plant Biol. **13:** 631–639.

Mathieu-Rivet, E., Gévaudant, F., Sicard, A., Salar, S., Do, P.T., Mouras, A., Fernie, A.R., Gibon, Y., Rothan, C., Chevalier, C., and Hernould, M. (2010). Functional analysis of the anaphase promoting complex activator CCS52A highlights the crucial role of endoreduplication for fruit growth in tomato. Plant J. **62:** 727–741.

Miller, J.J., Summers, M.K., Hansen, D.V., Nachury, M.V., Lehman, N.L., Loktev, A., and Jackson, P.K. (2006). Emi1 stably binds and inhibits the anaphase-promoting complex/cyclosome as a pseudosubstrate inhibitor. Genes Dev. **20:** 2410–2420.

Narbonne-Reveau, K., Senger, S., Pal, M., Herr, A., Richardson, H.E., Asano, M., Deak, P., and Lilly, M.A. (2008). APC/C$^{Fzr/Cdh1}$ promotes cell cycle progression during the *Drosophila* endocycle. Development **135:** 1451–1461.

Ohe, M., Inoue, D., Kanemori, Y., and Sagata, N. (2007). Erp1/Emi2 is essential for the meiosis I to meiosis II transition in *Xenopus* oocytes. Dev. Biol. **303:** 157–164.

Ohe, M., Kawamura, Y., Ueno, H., Inoue, D., Kanemori, Y., Senoo, C., Isoda, M., Nakajo, N., and Sagata, N. (2010). Emi2 inhibition of the anaphase-promoting complex/cyclosome absolutely requires Emi2 binding via the C-terminal RL tail. Mol. Biol. Cell **21:** 905–913.

Page, A.M., and Hieter, P. (1999). The anaphase-promoting complex: New subunits and regulators. Annu. Rev. Biochem. **68:** 583–609.

Pérez-Pérez, J.M., Serralbo, O., Vanstraelen, M., González, C., Criqui, M.-C., Genschik, P., Kondorosi, E., and Scheres, B. (2008). Specialization of CDC27 function in the *Arabidopsis thaliana* anaphase-promoting complex (APC/C). Plant J. **53:** 78–89.

Perilli, S., and Sabatini, S. (2010). Analysis of root meristem size development. Methods Mol. Biol. **655:** 177–187.

Peters, J.-M. (2002). The anaphase-promoting complex: Proteolysis in mitosis and beyond. Mol. Cell **9:** 931–943.

Pfleger, C.M., and Kirschner, M.W. (2000). The KEN box: An APC recognition signal distinct from the D box targeted by Cdh1. Genes Dev. **14:** 655–665.

Proost, S., Van Bel, M., Sterck, L., Billiau, K., Van Parys, T., Van de Peer, Y., and Vandepoele, K. (2009). PLAZA: A comparative genomics resource to study gene and genome evolution in plants. Plant Cell **21:** 3718–3731.

Reimann, J.D.R., Freed, E., Hsu, J.Y., Kramer, E.R., Peters, J.-M., and Jackson, P.K. (2001). Emi1 is a mitotic regulator that interacts with Cdc20 and inhibits the anaphase promoting complex. Cell **105:** 645–655.

Takahashi, N., Lammens, T., Boudolf, V., Maes, S., Yoshizumi, T., De Jaeger, G., Witters, E., Inzé, D., and De Veylder, L. (2008). The

DNA replication checkpoint aids survival of plants deficient in the novel replisome factor ETG1. EMBO J. **27:** 1840–1851.

Tang, Z., Li, B., Bharadwaj, R., Zhu, H., Özkan, E., Hakala, K., Deisenhofer, J., and Yu, H. (2001). APC2 Cullin protein and APC11 RING protein comprise the minimal ubiquitin ligase module of the anaphase-promoting complex. Mol. Biol. Cell **12:** 3839–3851.

Tategu, M., Nakagawa, H., Sasaki, K., Yamauchi, R., Sekimachi, S., Suita, Y., Watanabe, N., and Yoshid, K. (2008). Transcriptional regulation of human polo-like kinases and early mitotic inhibitor. J. Genet. Genomics **35:** 215–224.

Tsukaya, H. (2008). Controlling size in multicellular organs: Focus on the leaf. PLoS Biol. **6:** e174.

Tung, J.J., Hansen, D.V., Ban, K.H., Loktev, A.V., Summers, M.K., Adler III, J.R., and Jackson, P.K. (2005). A role for the anaphase-promoting complex inhibitor Emi2/XErp1, a homolog of early mitotic inhibitor 1, in cytostatic factor arrest of *Xenopus* eggs. Proc. Natl. Acad. Sci. USA **102:** 4318–4323.

Ullah, Z., Lee, C.Y., Lilly, M.A., and DePamphilis, M.L. (2009). Developmentally programmed endoreduplication in animals. Cell Cycle **8:** 1501–1509.

Van Leene, J., et al. (2007). A tandem affinity purification-based technology platform to study the cell cycle interactome in Arabidopsis thaliana. Mol. Cell. Proteomics **6:** 1226–1238.

Van Leene, J., et al. (2010). Targeted interactomics reveals a complex core cell cycle machinery in *Arabidopsis thaliana.* Mol. Syst. Biol. **6:** 397.

Vandepoele, K., Vlieghe, K., Florquin, K., Hennig, L., Beemster, G.T. S., Gruissem, W., Van de Peer, Y., Inzé, D., and De Veylder, L. (2005). Genome-wide identification of potential plant E2F target genes. Plant Physiol. **139:** 316–328.

Vanstraelen, M., Baloban, M., Da Ines, O., Cultrone, A., Lammens, T., Boudolf, V., Brown, S.C., De Veylder, L., Mergaert, P., and Kondorosi, E. (2009). APC/C-^{CCS52A} complexes control meristem maintenance in the *Arabidopsis* root. Proc. Natl. Acad. Sci. USA **106:** 11806–11811.

Verschuren, E.W., Ban, K.H., Masek, M.A., Lehman, N.L., and Jackson, P.K. (2007). Loss of Emi1-dependent anaphase-promoting complex/cyclosome inhibition deregulates E2F target expression and elicits DNA damage-induced senescence. Mol. Cell. Biol. **27:** 7955–7965.

Vodermaier, H.C., Gieffers, C., Maurer-Stroh, S., Eisenhaber, F., and Peters, J.-M. (2003). TPR subunits of the anaphase-promoting complex mediate binding to the activator protein CDH1. Curr. Biol. **13:** 1459–1468.

Zuo, J., Niu, Q.W., and Chua, N.H. (2000). Technical advance: An estrogen receptor-based transactivator XVE mediates highly inducible gene expression in transgenic plants. Plant J. **24:** 265–273.